Journal of Alloys and Compounds 993 (2024) 174576

Contents lists available at ScienceDirect

Journal of Alloys and Compounds

journal homepage: www.elsevier.com/locate/jalcom

Investigating the reversible nature of the magnetocaloric effect under cyclic conditions of the $Ni_{50}Mn_{34}In_{15}Ga_1$ magnetic shape memory alloy

P. Álvarez-Alonso [a,b,*], J.P. Camarillo-García [c], D. Salazar [d], J. López-García [a], C. Echevarria-Bonet [a], P. Lázpita [d], K. Padrón-Alemán [a,e], J.L. Sánchez Llamazares [a,f], H. Flores-Zúñiga [f], V. Chernenko [d,g]

[a] Departamento de Física, Universidad de Oviedo, Oviedo 33007, Spain
[b] Instituto Universitario de Tecnología Industrial de Asturias, Universidad de Oviedo, Gijón 33203, Spain
[c] Unidad Académica de Ingeniería I, Universidad Autónoma de Zacatecas, Ramón López Velarde 801, Col, Zacatecas, Centro 98000, Mexico
[d] Basque Center for Materials Applications and Nanostructures & University of Basque Country (UPV/EHU), Leioa 48940, Spain
[e] Institut Laue-Langevin, 71 Avenue des Martyrs, CS20156, Grenoble 38042 Cédex 9, France
[f] Instituto Potosino de Investigación Científica y Tecnológica A.C., Camino a la Presa San José 2055, Col. Lomas 4ª sección, San Luis Potosí SLP 78216, Mexico
[g] Ikerbasque, Basque Foundation for Science, Bilbao 48009, Spain

ARTICLE INFO

Keywords:
Magnetic shape-memory alloy
Martensitic transformation
Adiabatic magnetocaloric effect
Cyclic stability
T-FORC distributions analysis

ABSTRACT

This study explores the reversibility of the martensitic transformation (MT) and magnetocaloric (MC) response of the Ga-doped $Ni_{50}Mn_{35}In_{15}$ magnetic shape memory alloys (MSMAs) with a Heusler structure. The direct and reverse MT occurs between temperatures $T_M \approx 257$ K and $T_A \approx 266$ K, respectively. The large MC effects resulting from the magnetic-field-induced first-order MT render these materials promising for room-temperature magnetic refrigeration. On account of both a low thermal hysteresis of MT ($\Delta T_{hyst} = 4$ K) at a magnetic field of 2 T and a highly reproducible peak value of the adiabatic temperature change at MT ($|\Delta T_{ad}| \approx 1.3$ K for $\mu_0 H = 1.9$ T), $Ni_{50}Mn_{34}In_{15}Ga_1$ MSMA emerges as a benchmark material for studying a cyclic stability of MC effects. During the first magnetic switching cycle, a reduction of ΔT_{ad} at MT by approximately 1.3 is observed, significantly lower than the reported one for other MC materials undergoing similar first-order phase transitions. Subsequent cycles revealed a consistent stability of the magnetic-field-induced ΔT_{ad} even after more than 200 magnetic field switching cycles. These findings suggest a notable degree of reversibility of the MT in the studied MSMA, which was also confirmed in the present work by a Temperature-First Order Reverse Curve distribution analysis.

1. Introduction

Heusler-type Ni-Mn-X (X = Ga, In, Sb) magnetic shape memory alloys (MSMAs) have garnered global attention over the last three decades due to their multifunctionality, originated from a strong interplay between elastic and magnetic degrees of freedom associated with the martensitic transformation (MT) [1,2]. Extensive research has been conducted on significant applied subjects, such as superelasticity [3,4] or magnetoresistance [5,6], as well as on the development of novel types of actuators and sensors capitalizing on their exceptional recoverable strains and rapid magneto-mechanical response to external stimuli [7,8]. Particularly, Ni-Mn-X MSMAs, where X = In, Sn, or Sb, have also attracted considerable interest due to their outstanding inverse magnetocaloric (MC) response. MC material exhibits temperature changes owing to its magnetizing/demagnetizing under the applied/removal of a magnetic field. The primary application of this phenomenon lies in magnetic refrigeration, a more efficient and environmentally friendly cooling technology compared to conventional gas-based systems [9]. Incidentally, numerous other potential applications have been proposed over the past decade in the areas of energy conversion and medical technologies [10].

The significant difference in magnetization between the martensitic and austenitic phases across the field-induced MT results in some of the highest ever achieved values of the magnetic-field-induced magnetic entropy change ($|\Delta S_M|^{max}$) [11–13], positioning MSMAs among the most promising MC materials [9,14].

Despite these advantages, the development of MC materials for energy-related applications, such as magnetic refrigeration, heat

* Corresponding author at: Departamento de Física, Universidad de Oviedo, Oviedo 33007, Spain.
E-mail address: alvarezapablo@uniovi.es (P. Álvarez-Alonso).

https://doi.org/10.1016/j.jallcom.2024.174576
Received 26 October 2023; Received in revised form 19 April 2024; Accepted 20 April 2024
Available online 25 April 2024

pumping, energy harvesting, etc. [15], needs careful consideration. This encompasses not only a substantial MC response in terms of $|\Delta S_M|^{max}$ and/or adiabatic temperature changes (ΔT_{ad}), but also considers other factors, such as the operating temperature range and the cyclic repeatability of ΔT_{ad}. The applicability of MSMAs at room temperature is encouraged by the ease of adjusting MT through appropriate selection of their chemical compositions [16–19] and/or thermal treatments [20,21]. Whereas reporting ΔT_{ad} data has become a standard practice, exploring MSMAs behavior under cyclical magnetic fields is often overlooked [22]. However, when researchers explore this area, they commonly observe a significant decrease in ΔT_{ad} at MT, approximately 2.5 times lower, after the initial magnetic cycle. [23–26]; furthermore, there have been limited studies of the conditions required to achieve repeatable ΔT_{ad} over hundreds of thermodynamic cycles. The latter is crucial for assessing the functional stability of MC materials, particularly those undergoing first-order phase transitions (FOPT), as their performance can degrade due to fatigue, mainly triggered by the transformation volume changes during magnetic cycles. In this context, Gamzatov et al. demonstrated a progressive reduction of ΔT_{ad} to zero in the $Ni_{47}Mn_{40}Sn_{12.5}Cu_{0.5}$ Heusler alloy after 7 cycles of the magnetic field changes $\mu_0\Delta H$ [24]. Our study aims to provide valuable insights into monitoring the long-term cycling of ΔT_{ad} in Heuser-type MSMAs.

As already mentioned before, the research on the ternary Mn-enriched Ni-Mn-X (X = In, Sn, or Sb) MSMAs with a significant MC effect is highly active driven by their notable MT-related $|\Delta S_M|^{max}$ and $|\Delta T_{ad}|^{max}$ values [27]. On the other hand, the exploration of MC properties in quaternary Ni-Mn-In-Ga alloys has been limited, despite their high potential to fine-tune the MC response by leveraging an additional degree of freedom and enhancing mechanical and magnetic properties. It is well known that doping MSMAs results in materials with properties that deviate significantly from the parent material. In this context, Aksoy *et al.* [28,29] adjusted MT around room temperature by partially substituting In for Ga in $Ni_{50}Mn_{34}In_{14}Ga_2$. Remarkably, this alloy maintained a similar value of $|\Delta S_M|^{max}$ compared to the parent alloy $Ni_{50}Mn_{34}In_{16}$, which was approximately 8 $Jkg^{-1}K^{-1}$ for $\mu_0\Delta H = 5T$. Subsequently, a large $|\Delta S_M|^{max}$ of 35 $Jkg^{-1}K^{-1}$ at $\mu_o\Delta H = 5$ T was reported for $Ni_{50}Mn_{34.5}In_{12.5}Ga_3$ [30]. However, to the best of our knowledge, neither measurements of ΔT_{ad} nor reports on its cyclic stability have been provided for Ni-Mn-In-Ga MSMAs.

In the present work, we have explored the reproducibility of ΔT_{ad} in the $Ni_{50}Mn_{34}In_{15}Ga_1$ alloy under the influence of hundreds of switching magnetic field cycles, a factor closely linked to the reversibility of MT. To assess the degree of reversibility of MT, Temperature-First Order Reverse Curve (T-FORC) distributions have been utilized, an innovative technique designed for investigating phase transitions in materials featuring FOPT [31]. T-FORC analysis stems from an analogy with the well-established FORC method, used to study magnetization hysteresis through isothermal recoil *M-H* measurements within the irreversible area of the hysteresis loops. T-FORC analysis involves subjecting the material to a controlled thermal cycling process while applying a varying magnetic field. The combination of thermal and magnetic stimuli enables mapping the intricate details of temperature-driven FOPT in magnetic materials [31,32]. The current work pioneers the combination of T-FORC and ΔT_{ad} techniques to unveil the high reversibility nature of MT, demonstrating sustainable cycles for the inverse MC effect across hundreds of magnetic field switching cycles.

2. Experimental

Polycrystalline alloy with a nominal composition of $Ni_{50}Mn_{34}In_{15}Ga_1$ (hereafter denoted as NiMnInGa) was prepared by arc-melting high-purity elements ($\geq$ 99.9%). The resulting ingot was sealed in a quartz ampoule filled with ultra-high purity argon, annealed at 1173 K for 24 hours, and quenched into iced water. This annealing treatment is a standard procedure to promote a high-ordered $L2_1$ crystal structure [12].

The elemental chemical composition confirmed through Energy Dispersive Spectroscopy analysis conducted on a Hitachi TM3000 SEM, was found to be $Ni_{51.0}Mn_{33.5}In_{14.5}Ga_{1.0}$ ($\pm$0.5 at%). Differential Scanning Calorimetry (DSC) curves were recorded with a cooling and heating sweep rate of 10 $Kmin^{-1}$ using a TA-Q200 DSC instrument. The X-ray powder diffraction (XRD) pattern was collected at room temperature with a Bruker D8 Advance diffractometer operating at 30 kV and 20 mA, with a Cu radiation source (λ_{Cu} = 1.5418Å). The XRD data obtained were examined through Le-Bail analysis performed using the FullProf suite [33].

Magnetization measurements were carried out using vibrating sample magnetometry in a Dynacool® Quantum Design PPMS®. The thermomagnetic $M(T)$ curves were acquired under constant magnetic fields of 10 mT and 2 T with a sweeping temperature rate of 1.0 K/min.

The magnetic field-induced adiabatic temperature change, ΔT_{ad}, was recorded using the measuring setup described elsewhere [34]. The $\Delta T_{ad}(T)$ measurement protocol for the heating ramp included the following steps: (i) cooling the sample below the martensite finish temperature, T_{MF}, under zero magnetic field to ensure its reproducibility and to overcome any potential discrepancies in the ΔT_{ad} determination due to the thermal history (a detailed discussion on the effect of thermal protocol on the MC effect is provided in ref. [35]); (ii) heating the sample to the measuring temperature ($T_{measure}$); (iii) stabilizing the temperature and subsequently placing the sample in the magnetic field. The measurement protocol for the cooling ramp included the following steps: (i) heating the sample above the austenite finishing temperature, T_{AF}; (ii) applying the magnetic field by introducing the sample between the polar pieces of the electromagnet and, afterward, cooling it to $T_{measure}$; and (iii) once the temperature stabilized, removing the sample from the magnetic field. Cyclic variations in the sample temperature were achieved by (i) heating/cooling the sample to the initial temperature from a state of pure martensite/austenite and (ii) alternately introducing/removing the sample into/from the magnetic field of the electromagnet.

The experimental procedure for generating the T-FORC diagrams involved measuring magnetization (M) with respect to the temperature (T) starting from selected return temperatures (T_R) within the MT temperature range. The values of T_R were chosen from the opposite branch of the $M(T)$ hysteretic curve for recoil measurements. A reference temperature (T_S), corresponding to a pure phase significantly distant from the phase transformation and in the opposite direction of the recoil curve, was also selected. Then, with a static magnetic field applied, the magnetization recoil curve was measured by starting at T_S and gradually reaching the value of T_R. This process was iterated for each T_R.

The T-FORC distribution function (ρ) is defined as the second mixed derivative:

$$\rho(T, T_R) = \pm\frac{\partial^2 M(T, T_R)}{\partial T \partial T_R} \quad (1)$$

where to keep a correct distribution, negative or positive signs are used when T_R is located on the cooling or heating branch of the thermal hysteresis loop, respectively [36]. The resulting T-FORC distribution is typically represented using a coordinate system rotated with respect to the measuring and T_R temperatures. This system introduces new axes, T_u and T_h, which are related to the center and absolute width of the distribution, respectively [32]:

$$T_u = \frac{(T_R + T)}{2} - T_{center} \quad (2)$$

$$T_h = \frac{|T_R - T|}{2} \quad (3)$$

T_{center} is defined as half the sum of the temperatures at which the maximum of the first derivatives of the magnetization appears in each direction. This study determined the T-FORC distribution corresponding to the phase transformation during cooling for a fixed magnetic field of

2 T. The curves $M(T)$ were measured with experimental points recorded at intervals of 1 K and a sweeping rate of 1 K/min.

3. Results and discussion

3.1. Transformation behavior

DSC curves in Fig. 1(a) show exothermic and endothermic peaks corresponding to the direct and reverse MT occurring at temperatures $T_M \approx 257$ K and $T_A \approx 266$ K, respectively. The starting (S) and finishing (F) temperatures of the martensitic and austenitic transformations (T_{MS}, T_{MF}, T_{AS}, and T_{AF}) were determined using the standard two-tangent method [37], resulting in values of 263, 250, 260, and 272 K, respectively. It is worth noting that the MT for parental $Ni_{50}Mn_{34}In_{16}$ alloy occurs at lower temperatures ($T_M \approx 230$ K and $T_A \approx 240$ K [38]), so the increase of MT temperatures in the studied alloy can be attributed to the Ga-doping (see also Refs. [28,29]). The alloy exhibits a low ΔT_{hyst} of 9 K, consistent with values reported for parental and similar alloys [30,38]. The transformation enthalpy (ΔH) and entropy change (ΔS) equals 5.3 Jg^{-1} and 20.2 $Jkg^{-1}K^{-1}$, respectively, in agreement with the reported data for the alloys of similar composition [39]. The inflection point observed on DSC curve [40] reveals the value of Curie temperature of austenite, T_C^A, equal to 301 K. This value is similar to that of the parental $Ni_{50}Mn_{34}In_{16}$ alloy [38], suggesting that the used Ga-doping has a minimal effect on the ferro-to-paramagnetic transition.

Fig. 1(b) illustrates the room temperature XRD pattern with Bragg peaks corresponding to the cubic austenite. Notably, in NiMn-based Heusler alloys, the austenite phase can exhibit either a highly ordered $L2_1$ or a less ordered B2 crystal structure, depending on thermal treatment [41] and/or synthesis conditions [42]. The appearance of the (111) reflection in the pattern is a standard criterion for distinguishing between both structures. The (111) reflection confirms that the alloy exhibits the $L2_1$ structure with a lattice parameter of 5.994(1) Å. Similar results have been found for the $Ni_{50}Mn_{34}In_{16-x}Ga_x$ and $Ni_{50}Mn_{33}In_{17-x}Ga_x$ alloys [19,43], as well as for the austenite phase in the undoped $Ni_{50}Mn_{35}In_{15}$ alloy.

The thermomagnetic $M(T)$ curve under a field of 10 mT is depicted in Fig. 1(c). During the cooling process, after the expected raising of the magnetization due to the paramagnetic-to-ferromagnetic transition, the magnetization begins to decline at $T_{MS}^{10mT} \approx 261$ K, a temperature close to the T_{MS} value obtained from the DSC data. This indicates the onset of the direct MT from the ferromagnetic austenite to the antiferromagnetic-like martensitic phase, as commonly occurs in ternary Ni-Mn-In alloys [1,44]. As the temperature further decreases, magnetization sharply drops to nearly zero at T_{MF}. Below 240 K, a transition occurs from the antiferromagnetic-like to ferrimagnetic states, and the transition temperature (tentatively referred to as the Curie temperature of the martensitic phase, T_C^M) is determined to be $T_C^M \approx 235$ K. This behavior is in line with earlier reports for $Ni_{50}M_{35}In_{15}$ alloy [44,45]. Upon heating, the reverse MT takes place between T_{AS} and T_{AF}.

Fig. 1(c) also depicts two successively recorded $M(T)$ curves under a magnetic field of 2 T. The curves are well matched, indicating the good repeatability of the magnetostructural phase transformation driven by temperature. MT shifts to lower temperatures under the influence of the magnetic field as a consequence of the metamagnetic character of the alloy [46]. Also, a prominent finding is a substantial reduction in ΔT_{hyst}, from 7 K at 10 mT to 4 K at 2 T, measured between the middle points of the MT loops. The magnetic field-induced reduction of ΔT_{hyst} can also be found in the Ni-Mn-Sn alloy [46], while the Ni-Mn-In alloy exhibits the opposite behavior [47]. The origin of the magnetic field-driven reduction of hysteresis in the studied NiMnInGa and cited Ni-Mn-Sn metamagnetic alloys needs separate purposeful study. However, in the present investigation, as a preliminary assumption, we suggest that this effect is related to a partial transformation owing to a well-known effect of the magnetic field-induced thermal arrest of a certain volume fraction of austenitic phase in MSMAs (see [48] and references therein). The aforementioned small and reproducible value of ΔT_{hyst} at 2 T is an important discovery that allows to consider the studied metamagnetic NiMnInGa alloy as a suitable model for investigating the variation of ΔT_{ad} under periodic magnetic field switching.

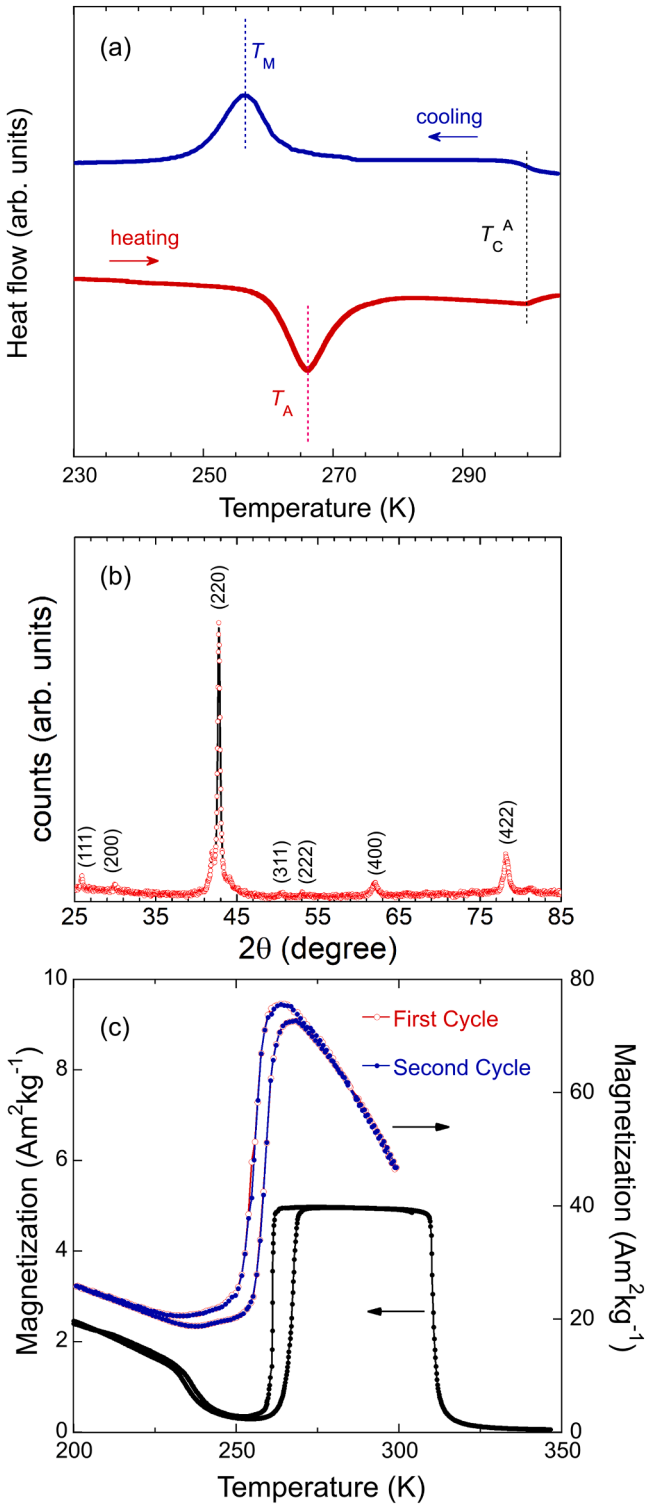

Fig. 1. (a) DSC heating and cooling runs. The characteristic temperatures of MT, T_M and T_A, as well as T_C^A, are indicated by the vertical dashed lines. (b) Room-temperature powder XRD pattern showing an $L2_1$-ordered cubic structure. (c) Thermomagnetization curves measured under a static magnetic field $\mu_0 H = 10$ mT (black circles) and recorded twice under a static magnetic field $\mu_0 H = 2$ T (red and blue).

3.2. Field-induced adiabatic temperature change

Fig. 2 depicts the dependencies of $\Delta T_{ad}(T)$ for magnetic field changes of 0.0–1.5 T and 0.0–1.9 T, following the cooling and heating protocols described in the experimental section. The graphs reveal a narrow peak followed by a broad one associated with MT and the second-order magnetic phase transition (SOMPT), respectively. As expected, the peaks at the MT temperatures on the cooling and heating branches exhibit a ΔT_{hyst} of around 5 K. In contrast, those related to SOMPT do not show hysteresis (as portrayed in the $M(T)^{2\ T}$ curves in Fig. 1(c)). Fig. 2 demonstrates that the change in $\mu_0 H$ from 1.5 T to 1.9 T impacts the $\Delta T_{ad}(T)$ peak positions, causing a slight reduction in the MT hysteresis. Moreover, as anticipated, the increase in the magnetic field change leads to an enlargement of the maximum adiabatic temperature change values: $\Delta T_{ad}^{1.5\ T}(253\ K) = 1.1$ K and $\Delta T_{ad}^{1.9\ T}(254\ K) = 1.3$ K when measured during cooling, and $\Delta T_{ad}^{1.5\ T}(259\ K) = -0.9$ K and $\Delta T_{ad}^{1.9\ T}(258\ K) = -1.1$ K during the heating. These values are larger and occur at higher temperatures compared to those of the parental $Ni_{50}Mn_{34}In_{16}$ alloy [49]. This is consistent with the observed shift to higher temperatures of the MT with the addition of Ga. Table 1 compiles our results and the values of $|\Delta T_{ad}|^{max}$ and $|\Delta T_{ad}/\mu_0\Delta H|$ reported in the literature for similar Mn-enriched Heusler MSMAs. The $|\Delta T_{ad}/\mu_0\Delta H|$ value for $Ni_{50}Mn_{34}In_{15}Ga_1$ surpasses the average in this category of compounds. Although the values of ΔT_{ad} are moderate compared to those of some other NiMn-based Heusler alloys, our material exhibits a sustainable ΔT_{ad} value (see cycling results in Section 3.3), which is relevant for developing heat exchanger prototypes.

Furthermore, Fig. 2 shows that regardless of the thermal protocol, the sign of the ΔT_{ad} peaks associated with the field-induced MT and SOMPT are opposite when $\mu_0 H$ changes from 0 T to 1.9 T or vice versa. To provide better visualization of the impact of the $\mu_0\Delta H$ change direction on the sample temperature variation, Fig. 3 offers typical time-dependent temperature profiles near T_C^A. The specimen is initially stabilized at zero magnetic field in the first testing cycle (indicated by the red oscillations in Fig. 3). Upon placement in a uniform magnetic field region of the electromagnet, the sample's temperature reaches its maximum (as demonstrated by the first peak in the red oscillations). Upon removal of the specimen from the electromagnet gap, its temperature decreases sharply (as observed, for instance, from the temperature reduction following the first maximum in the red oscillations in Fig. 3). Conversely, when the specimen is initially placed in a magnetic field and then rapidly removed from it, the specimen cools down (see, for instance, the first cycle of the blue section of the oscillations in Fig. 3).

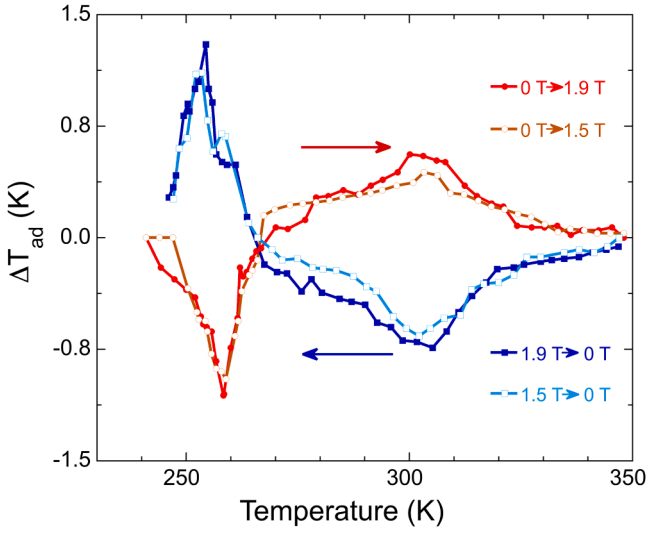

Fig. 2. $\Delta T_{ad}(T)$ curves measured under magnetic field changes of 1.5 T and 1.9 T across the first-order magnetostructural and second-order magnetic transitions. Different heating/cooling protocols for the magnetic field changes have been used (see text for details).

Table 1
Maximum values of $|\Delta T_{ad}|$ and $|\Delta T_{ad}/\mu_0\Delta H|$ observed near MT obtained in the present work and reported for other bulk NiMn-based Heusler-type MSMAs.

Alloy	$\mu_0\Delta H$ (T)	$\lvert\Delta T_{ad}^{M\text{-}A}\rvert$ (K)	$\lvert\Delta T_{ad}/\mu_0\Delta H\rvert$ (K/T)	$\lvert\Delta T_{ad}^{A\text{-}M}\rvert$ (K)	$\lvert\Delta T_{ad}/\mu_0\Delta H\rvert$ (K/T)	Ref.
$Ni_{45.2}Mn_{36.7}In_{13}Co_{5.1}$	0–2	6.2	3.1	-	-	[56]
$Ni_{50}Mn_{34}In_{14}Ga_1$	0–1.9	1.1	0.6	-	-	This
	1.9–0	-	-	1.3	0.7	work
$Ni_{50}Mn_{35}In_{14}Al_1$	0–1.8	1.8	1.0	-	-	[57]
$Ni_{50}Mn_{35}In_{14}Ge_1$	0–1.8	1.5	0.8	-	-	[57]
$Ni_{50}Mn_{34.8}In_{14.2}B$	0–1.8	1.5	0.8	-	-	[58]
$Ni_{50.0}Mn_{35.3}In_{14.7}$	0–5	2	0.4	-	-	[59]
	5–0	-	-	1.1	0.2	
$Ni_{50}Mn_{35}In_{15}$	0–20	7.0	0.4	-	-	[60]
	0–1.8	1.8	1.0	-	-	[57]
$Ni_{49.8}Mn_{35}In_{15.2}$	0–2	5.2	2.6	-	-	[56]
$Ni_{50.4}Mn_{34.8}In_{15.8}$	0–2	3.6	1.8	-	-	[56]
$Ni_{50}Mn_{34}In_{16}$	0–1.3	0.6	0.5	-	-	[49]
$Ni_{47}Mn_{40}Sn_{12.5}Cu_{0.5}$	0–1.8	0.6	0.3			[24]
$Ni_{50}Mn_{36}Sn_{13}Co_1$	0–1.93	0.8	0.4	0.3	0.2	[51]
$Ni_{50}Mn_{35}Sn_{15}$	0–8	3.9	0.5	-	-	[61]
$Ni_{48.6}Mn_{34.9}Sn_{16.5}$	0–5	2.6	0.5	-	-	[59]
	5–0	-	-	0.5	0.1	
$Ni_{55.3}Mn_{19.3}Ga_{25.4}$	0–1.93	1.0	0.5	1.5	0.8	[52]
$Ni_{45}Mn_{38}Sb_{12}Co_5$	0–20	10.2	0.5	11.3	0.6	[53]

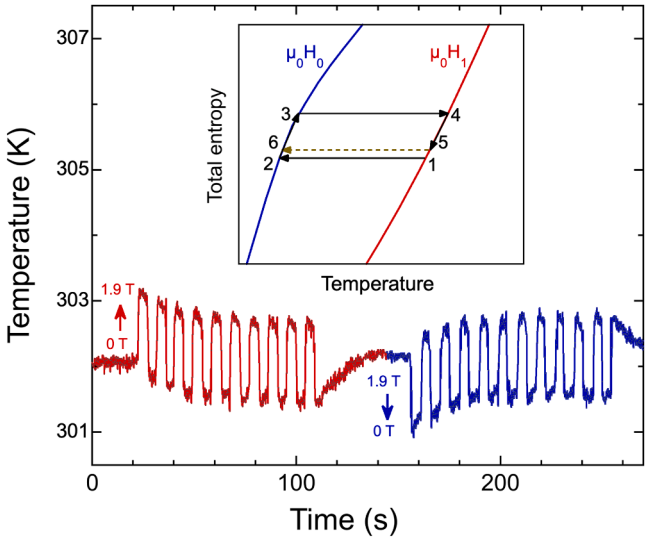

Fig. 3. Sample temperature near T_C^A as a function of time upon the cyclical variation of the magnetic field. Red oscillations: the temperature was stabilized without a magnetic field; blue oscillations: the temperature was stabilized under applied magnetic field $\mu_0 H = 1.9$ T. Inset: schematic representation of the temperature dependence of the total entropy, *S*, under two different magnetic fields $\mu_0 H_1 > \mu_0 H_0$.

Fig. 3 reveals that cycling the magnetic field leads to a drift in the initially stabilized temperature (302 K) until the fifth cycle, as observed in the red and blue oscillations. However, the drift diminishes with further cycling, and the average sample temperature becomes stable. This behavior aligns with the reported one in Ref. [50]. The observed drift is due to the limitations of the measuring setup. The inset of Fig. 3, in which the MC behavior near T_C^A is schematically illustrated using the total entropy, S_T, versus *T* diagram, portrays the following process: after temperature stabilization at the point (1), a reduction of the magnetic field from $\mu_0 H_1$ to $\mu_0 H_0$ (corresponding to the oscillating blue curve)

entails a decrease in the specimen temperature. After that, as the magnetic field remains constant for 4 seconds, a heat exchange with the environment raises the temperature [schematized in the process (2)→(3) in the inset of Fig. 3]. Furthermore, an increase in the magnetic field yields the temperature change observed in the process (3)→(4). Then, while the magnetic field is held constant [represented as the path (4)→(5)], the heat exchange between the sample and the environment reduces the temperature. It is worth noting that, although we have assumed the same temperature variation in processes (2)→(3) and (4)→(5) in the S_T-T diagram, there is a net temperature increment along the cycle, i.e., when the specimen is extracted again from the magnetic field [path (5)→(6)] the temperature change differs from that one corresponding to the process (1)→(2). Reversing the cycle from (6) to (1) reduces the net temperature, which is consistent with the behavior of the oscillating red curve shown in Fig. 3.

It is evident from Fig. 2 that the maximum values of $\Delta T_{ad}(T)$ on the cooling and heating curves exhibit mirror-like positions with each other at SOMPT, supporting the nonhysteretic nature of the magnetic phase transition. In contrast, the $\Delta T_{ad}(T)$ peaks associated with the direct and reverse MT occur at different temperatures due to the MT hysteresis and its sensitivity to the magnetic field. However, the values of $|\Delta T_{ad}|^{max}$, about 1.3 K at a magnetic field change of 1.9 T, exhibit a high degree of proximity, differing only by 10%, for the direct MT during the cooling run and for the reverse MT during the heating process. This finding differs from the behavior observed in other NiMn-based MSMA (see, for instance, Refs. [51–53]), where this difference is considerably bigger and highly influenced by the width of the temperature hysteresis and the magnetic field dependence of the MT temperatures [54]. A good matching of the values underscores a significant reversibility of MT in the studied $Ni_{50}Mn_{34}In_{15}Ga_1$ alloy. This reversibility may be attributed to the reduced thermal hysteresis of MT, which is further almost halved under a magnetic field of about 2 T, as disclosed in this work.

3.3. Cyclic stability of adiabatic temperature change in the vicinity of MT

Building on the previous section's findings, we analyze the MC material's performance in magnetic-field cycling (0.0 T↔1.9 T) experiments at various reference temperatures. In the cycling measurements of ΔT_{ad} within the SOMPT region (not shown), there is a continuous variation in the maximum/minimum values for the first 5–10 cycles before reaching stabilization. Additionally, a gradual thermal fluctuation (approximately 0.5 K) occurs over an extended period, likely stemming from environmental temperature fluctuations, as previously addressed.

Fig. 4 illustrates the switching magnetic field-induced temperature changes of the sample measured in the MT regions as a function of time. Before initiating the measurements related to the reverse MT, the specimen was cooled below T_{MF} and then heated to 256.5 K, a temperature proximate to the $|\Delta T_{ad}|$ peak during the reverse MT. The exemplified results of these measurements are depicted by the blue oscillations in Fig. 3. When engaging the forward MT, the sample was initially heated above T_{AF}, then cooled under a magnetic field of 1.9 T to 254 K, close to the $|\Delta T_{ad}|$ peak at the direct MT in Fig. 2. Subsequently, the sample was subjected to cycling, as shown by the selected red oscillations. In the initial condition, the first application or removal of the magnetic field yields ΔT_{ad} values with opposite signs. This behavior reflects an inverse MC effect at MT, in contrast to the conventional MC effect observed during SOMPT (Fig. 3).

Note that the amplitude of ΔT_{ad} corresponding to the first magnetic cycle, as indicated by dashed lines in Fig. 4, consistently surpasses that one observed in the following cycles. This fact suggests that not all the material transforms back into its initial phase state before the first cycle. In contrast to the usual 2.5 times reduction observed in other NiMn-based Heusler alloys [24–26], our alloy showcases a reduction of about 1.3 times, unveiling unique and promising characteristics. In this sense, the subsequent multitude oscillations reveal a reproducible cyclic

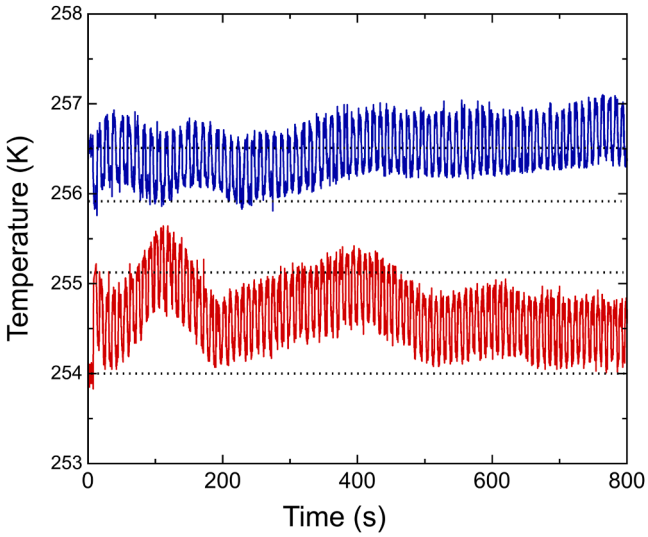

Fig. 4. Time dependences of the cyclical magnetic field induced adiabatic temperature change across the reverse MT after the specimen was cooled to $T < T_{MF}$ under zero magnetic field and then heated to a test temperature (blue oscillations); and across the forward MT after the specimen was heated to $T > T_{AF}$ and then cooled under a magnetic field of 1.9 T to a test temperature (red oscillations).

behavior, with amplitude stabilization occurring after some time, regardless of the thermal protocol used. Note that the extensive use of magnetic field switching cycles in this study (more than 200 cycles) exceeds by almost an order of magnitude those reported in the literature for other NiMn-based MSMAs, typically limited to a few tens of cycles. Long-term cycling is crucial to ensuring samples' mechanical stability (and, consequently, magnetic stability) in functional applications. The results show that the Ga-doped Ni50Mn35In15 system is promising for implementation in refrigerant prototypes, facilitating an analysis of the long-term MC performance of MSMAs.

Additionally, it is noteworthy that the cycling process increases the average sample temperature, typically by 0.5 K. The prominent finding from the observed behavior in Fig. 4 for both measurement protocols is the affirmation of the reversible character of the magnetic field-induced MT. Once a steady state of periodic $|\Delta T_{ad}|$ is achieved, the MC response becomes nearly identical for the direct and reverse MT. This is because, in both cases, a similar volume fraction of the sample participates in the repeated reversible transformation between the austenitic and martensitic phases. Such a behavior differs from the results on Ni-Mn-Sn-Co MSMA, where a continuous reduction of $|\Delta T_{ad}|$ was observed due to a gradual decrease of the volume fraction of the martensitic phase involved in the cycling across MT [24].

3.4. T-FORC analysis of MT

Fig. 5(a) shows the major hysteresis loop of MT and the minor reverse curves for a magnetic field of 2 T. Fig. 5(b) illustrates the T-FORC distribution of this phase transformation as generated from the partial derivatives of the reverse curves (see Eq. (1)) without using any smoothing methods. As a result, certain sections of the diagram exhibit experimental noise, but the dominant regions are clearly defined. The most significant positive values of the distribution are linked to the temperatures near the maximum change rate of the $M(T)$ curve. The distribution features the following four regions: (1) an approximately circular area encompassing the maximum distribution values, occurring for T_R between 255 and 259 K, i.e., within the mixed phase region, which has been associated with a symmetrical martensitic transformation [36]. (2) An elongation to the right of the zone (1) in a 45° direction, associated with higher T_R values (> 259 K), reflecting the

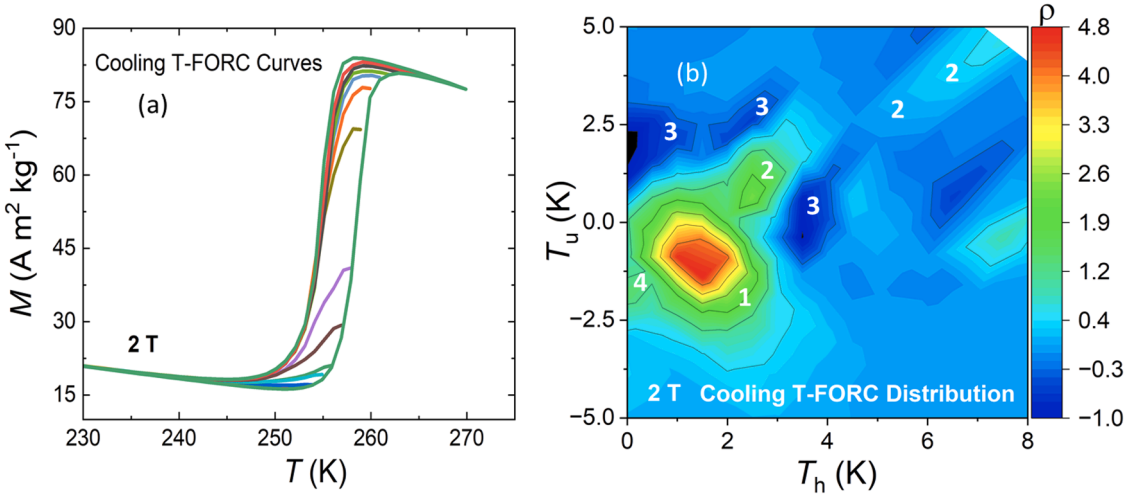

Fig. 5. (a) Major thermal hysteresis loops of MT and T-FORC recoil curves in the cooling protocol for a static magnetic field of 2 T. (b) T-FORC distribution of the martensitic transformation at 2 T.

challenges faced by the remaining martensitic phase transforming into the austenite phase [55]. (3) Negative values in the distribution can be interpreted as a non-uniformity in the transformed austenite phase during heating due to the influence of T_C^A, as described in [55]. (4) A small tail opposite to the area (2). In this area, T_R curves commence with remnants of the austenite phase. The slight shift in the distribution center towards negative T_u values likely represents the principal changes between the reverse curves' endpoints when the martensite becomes the predominant phase.

4. Summary

We have investigated the reversibility of the martensitic transformation (MT) in the low-hysteresis polycrystalline $Ni_{50}Mn_{34}In_{15}Ga_1$ magnetic shape memory alloy. This alloy exhibits a $L2_1$-ordered cubic austenitic structure at room temperature and undergoes a magnetostructural MT with martensitic and austenitic temperatures of $T_M \approx 257$ K and $T_A \approx 266$ K, respectively. Application of a magnetic field induces a shift of the MT to lower temperatures and a significant reduction in the thermal hysteresis, down to about 4 K under a magnetic field of 2 T.

The temperature dependence of the magnetic field-induced adiabatic temperature change ΔT_{ad} reveals two distinct peaks corresponding to the MT temperature (T_M, T_A) and the curie temperature of the austenite T_C^A. Under an applied magnetic field of 1.9 T, the magnitudes of $|\Delta T_{ad}|$ were approximately 0.7 K at T_C^A and 1.3 K near (T_M, T_A) for both heating and cooling protocols.

The reduced hysteresis width and the similarity in $|\Delta T_{ad}|$ amplitudes near both T_M and T_A underscore the high degree of reversibility of the thermally and magnetically induced martensitic transformation. This encouraged a first-ever investigation into the long-term cycling behavior of $|\Delta T_{ad}|$ with a varying magnetic field in MSMAs. The results reveal a stabilization trend of the volume fraction of reversibly transformed material with a large number of cycles, opening the door for the utilization of the Ni-Mn-In-Ga quaternary alloys for heat exchanger prototypes suitable for studying their long-term thermal and magnetic stabilities.

The application of the T-FORC distribution technique was found to be successful in obtaining unique insights into MT behavior, revealing four distinct regions and shedding light on the transformation characteristics of this alloy, particularly within the mixed-phase region associated with the inverse magnetocaloric response.

In summary, high reversibility of the metamagnetic-type MT in $Ni_{50}Mn_{34}In_{15}Ga_1$, coupled with the essential value of sustainable adiabatic temperature change under easily accessible values of the magnetic field, positions it favorably for future proof-of-concept MC applications.

Declaration of Competing Interest

The authors declare the following financial interests/personal relationships which may be considered as potential competing interests: Pablo Alvarez Alonso reports financial support, article publishing charges, equipment, drugs, or supplies, and travel were provided by Spanish Ministerio de Ciencia e Innovación. Cristina Echevarria Bonet reports financial support and equipment, drugs, or supplies were provided by Asturian government. Horacio Flores Zuniga reports financial support was provided by Laboratorio Nacional de Nanociencias y Nanotecnologia. Daniel Salazar Jaramillo reports financial support, equipment, drugs, or supplies, and travel were provided by Basque Government. Jose Luis Sanchez Llamazares reports financial support and travel were provided by Spanish Ministerio de Universidades. Kenny Padron Aleman reports was provided by Institut Laue-Langevin. Volodymyr Chernenko reports equipment, drugs, or supplies was provided by University of the Basque Country - Bizkaia Campus. If there are other authors, they declare that they have no known competing financial interests or personal relationships that could have appeared to influence the work reported in this paper.

Data Availability

Data will be made available on request.

Acknowledgments

The support received from the following organizations is gratefully acknowledged: Spanish MCIN/AEI/10.13039/501100011033/ and ERDF, UE (project number: PID2022–138256NB-C21, PID2022–138256NA-C22, and PID2022-138108OB-C33), Asturian government, and European FEDER (project: AYUD/2021/51822), Laboratorio Nacional de Nanociencias y Nanotecnologia (LINAN, IPICyT, Mexico), and the Basque Government Department of Education (project: IT1479–22). J.L. Sánchez Llamazares acknowledges the support received from the European Union-NextGenerationEU, and Spanish Ministerio de Universidades and Plan de Recuperación, Transformación y Resiliencia, in the framework of the Maria Zambrano program of the University of Oviedo, Asturias, Spain (Reference: MU-21-UP2021–030 71741542; that made possible his 2023–2022 sabbatical stay at Uniovi).

K. Padrón-Alemán acknowledges the Institute Laue-Langevin for his PhD/CFR contract (Reference: ESP-5–2023). The authors are thankful to I. Orue, from the technical service of the University of the Basque Country.

References

[1] Y. Sutou, Y. Imano, N. Koeda, T. Omori, R. Kainuma, K. Ishida, K. Oikawa, Magnetic and martensitic transformations of NiMnX(X=In, Sn, Sb) ferromagnetic shape memory alloys, Appl. Phys. Lett. 85 (2004) 4358–4360, https://doi.org/10.1063/1.1808879.

[2] A. Zhukov, Novel Functional Magnetic Materials, Springer International Publishing, Cham, 2016, https://doi.org/10.1007/978-3-319-26106-5.

[3] T.-F.F.M. Chang, V. Chernenko, H.C. Tang, C.Y. Chen, A. Umise, M. Tahara, H. Hosoda, M. Sone, Superelastic behavior of single crystalline Ni48Fe20Co5Ga27 micro-pillars near austenite-martensite critical point, AIP Adv. 11 (2021) 25213, https://doi.org/10.1063/5.0036304.

[4] C. Lauhoff, A. Reul, D. Langenkämper, P. Krooß, C. Somsen, M.J. Gutmann, B. Pedersen, I.V. Kireeva, Y.I. Chumlyakov, G. Eggeler, W.W. Schmahl, T. Niendorf, Effects of aging on the stress-induced martensitic transformation and cyclic superelastic properties in Co-Ni-Ga shape memory alloy single crystals under compression, Acta Mater. 226 (2022) 117623, https://doi.org/10.1016/j.actamat.2022.117623.

[5] Y. Wu, H. Xuan, S. Agarwal, Y. Xu, T. Zhang, L. Feng, H. Li, P. Han, C. Zhang, D. Wang, F. Chen, Y. Du, Large magnetocaloric effect and magnetoresistance in Fe and Co Co-Doped Ni-Mn-Al Heusler Alloys, Phys. Status Solidi (A) Appl. Mater. Sci. 215 (2018) 1700843, https://doi.org/10.1002/pssa.201700843.

[6] X.M. Huang, Y. Zhao, H. Le Yan, N. Jia, B. Yang, Z. Li, Y. Zhang, C. Esling, X. Zhao, L. Zuo, Giant magnetoresistance, magnetostrain and magnetocaloric effects in a Cu-doped<001>-textured Ni45Co5Mn36In13.2Cu0.8 polycrystalline alloy, J. Alloy. Compd. 889 (2021) 161652, https://doi.org/10.1016/j.jallcom.2021.161652.

[7] H. Shi, Z. Liu, H. Wang, X. Mei, Design and performance analysis of hydraulic switching valve driven by magnetic shape memory alloy, Adv. Mech. Eng. 13 (2021) 1–15, https://doi.org/10.1177/16878140211016985.

[8] A.M. Davis, M.M. Mirsayar, D.J. Hartl, A novel structural health monitoring approach in concrete structures using embedded magnetic shape memory alloy components, Constr. Build. Mater. 311 (2021) 125212, https://doi.org/10.1016/j.conbuildmat.2021.125212.

[9] V. Franco, J.S.S. Blázquez, J.J.J. Ipus, J.Y.Y. Law, L.M.M. Moreno-Ramírez, A. Conde, Magnetocaloric effect: from materials research to refrigeration devices, Prog. Mater. Sci. 93 (2018) 112–232, https://doi.org/10.1016/j.pmatsci.2017.10.005.

[10] A.M. Tishin, Y.I. Spichkin, V.I. Zverev, P.W. Egolf, A review and new perspectives for the magnetocaloric effect: new materials and local heating and cooling inside the human body, Int. J. Refrig. 68 (2016) 177–186, https://doi.org/10.1016/j.ijrefrig.2016.04.020.

[11] X. Zhou, H. Kunkel, G. Williams, S. Zhang, X. Desheng, Phase transitions and the magnetocaloric effect in Mn rich Ni-Mn-Ga Heusler alloys, J. Magn. Magn. Mater. 305 (2006) 372–376, https://doi.org/10.1016/j.jmmm.2006.01.029.

[12] C.O. Aguilar-Ortiz, J.P. Camarillo-García, J. Vergara, P. Álvarez-Alonso, D. Salazar, V.A. Chernenko, H. Flores-Zúñiga, Effect of solidification rate on martensitic transformation behavior and adiabatic magnetocaloric effect of Ni50Mn35In15 ribbons, J. Alloy. Compd. 748 (2018) 464–472, https://doi.org/10.1016/j.jallcom.2018.03.074.

[13] A. Deltell, A.E.-M.A. Mohamed, P. Álvarez-Alonso, M. Ipatov, J.P. Andrés, J. A. González, T. Sánchez, A. Zhukov, M.L. Escoda, J.J. Suñol, R. López Antón, Martensitic transformation, magnetic and magnetocaloric properties of Ni–Mn–Fe–Sn Heusler ribbons, J. Mater. Res. Technol. 12 (2021) 1091–1103, https://doi.org/10.1016/j.jmrt.2021.03.049.

[14] V.A. Chernenko, V.A. L'vov, E. Cesari, J.M. Barandiaran, Fundamentals of magnetocaloric effect in magnetic shape memory alloys, in: E. Brück (Ed.), Handbook of Magnetic Materials, 2019: pp. 1–45. https://doi.org/10.1016/bs.hmm.2019.03.001.

[15] A. Kitanovski, Energy applications of magnetocaloric materials, Adv. Energy Mater. 10 (2020) 1903741, https://doi.org/10.1002/aenm.201903741.

[16] X. Moya, L. Mañosa, A. Planes, T. Krenke, M. Acet, E.F. Wassermann, Martensitic transition and magnetic properties in Ni–Mn–X alloys, Mater. Sci. Eng.: A 438–440 (2006) 911–915, https://doi.org/10.1016/j.msea.2006.02.053.

[17] A. Planes, L. Mañosa, M. Acet, Magnetocaloric effect and its relation to shape-memory properties in ferromagnetic Heusler alloys, J. Phys. Condens. Matter 21 (2009) 233201, https://doi.org/10.1088/0953-8984/21/23/233201.

[18] N.V. Rama Rao, V. Chandrasekaran, K.G. Suresh, Effect of Ni/Mn ratio on phase transformation and magnetic properties in Ni-Mn-In alloys, J. Appl. Phys. 108 (2010) 043913, https://doi.org/10.1063/1.3467966.

[19] Z.H. Liu, G.T. Li, Z.G. Wu, X.Q. Ma, Y. Liu, G.H. Wu, Tailoring martensitic transformation and martensite structure of NiMnIn alloy by Ga doping In, J. Alloy. Compd. 535 (2012) 120–123, https://doi.org/10.1016/j.jallcom.2012.04.088.

[20] V. Recarte, J.I. Pérez-Landazábal, V. Sánchez-Alarcos, V. Zablotskii, E. Cesari, S. Kustov, Entropy change linked to the martensitic transformation in metamagnetic shape memory alloys, Acta Mater. 60 (2012) 3168–3175, https://doi.org/10.1016/j.actamat.2012.02.022.

[21] V. Recarte, J.I. Pérez-Landazábal, V. Sánchez-Alarcos, J.A. Rodríguez-Velamazán, Dependence of the martensitic transformation and magnetic transition on the atomic order in Ni-Mn-In metamagnetic shape memory alloys, Acta Mater. 60 (2012) 1937–1945, https://doi.org/10.1016/j.actamat.2012.01.020.

[22] K. Wang, Y. Ouyang, Y. Shen, Y. Zhang, M. Zhang, J. Liu, High-throughput characterization of the adiabatic temperature change for magnetocaloric materials, J. Mater. Sci. 56 (2021) 2332–2340, https://doi.org/10.1007/s10853-020-05403-x.

[23] A.G. Gamzatov, A.B. Batdalov, S.K. Khizriev, A.M. Aliev, A.G. Varzaneh, P. Kameli, The nature of the frequency dependence of the adiabatic temperature change in Ni50Mn28Ga22-x(Cu, Zn)x Heusler alloys in cyclic magnetic fields, J. Alloy. Compd. 965 (2023) 171451, https://doi.org/10.1016/j.jallcom.2023.171451.

[24] A.G. Gamzatov, A.M. Aliev, A. Ghotbi Varzaneh, P. Kameli, I.A. Sarsari, S.C. Yu, Inverse-direct magnetocaloric effect crossover in Ni47Mn40Sn12.5Cu0.5 Heusler alloy in cyclic magnetic fields, Appl. Phys. Lett. 113 (2018) 0–5, https://doi.org/10.1063/1.5049398.

[25] T. Gottschall, K.P. Skokov, F. Scheibel, M. Acet, M.G. Zavareh, Y. Skourski, J. Wosnitza, M. Farle, O. Gutfleisch, Dynamical effects of the martensitic transition in magnetocaloric heusler alloys from direct δtad measurements under different magnetic-field-sweep rates, Phys. Rev. Appl. 5 (2016) 024013, https://doi.org/10.1103/PhysRevApplied.5.024013.

[26] T. Gottschall, K.P. Skokov, B. Frincu, O. Gutfleisch, Large reversible magnetocaloric effect in Ni-Mn-In-Co, Appl. Phys. Lett. 106 (2015) 021901, https://doi.org/10.1063/1.4905371.

[27] G.H. Yu, Y.L. Xu, Z.H. Liu, H.M. Qiu, Z.Y. Zhu, X.P. Huang, L.Q. Pan, Recent progress in Heusler-type magnetic shape memory alloys, Rare Met. 34 (2015) 527–539, https://doi.org/10.1007/s12598-015-0534-1.

[28] S. Aksoy, T. Krenke, M. Acet, E.F. Wassermann, X. Moya, L. Mañosa, A. Planes, Tailoring magnetic and magnetocaloric properties of martensitic transitions in ferromagnetic Heusler alloys, Appl. Phys. Lett. 91 (2007) 241916, https://doi.org/10.1063/1.2825283.

[29] M.Sc Seda Aksoy, Magnetic interactions in martensitic Ni-Mn based Heusler systems, Universität Duisburg-Essen, 2010.

[30] A.Y. Takeuchi, C.E. Guimarães, E.C. Passamani, C. Larica, Enhancement of magnetocaloric properties near room temperature in Ga-doped Ni50Mn34.5In15.5 Heusler-type alloy, J. Appl. Phys. 111 (2012) 103902, https://doi.org/10.1063/1.4716033.

[31] V. Franco, Temperature-FORC analysis of a magnetocaloric Heusler alloy using a unified driving force approach (T*FORC), J. Appl. Phys. 127 (2020), https://doi.org/10.1063/5.0005076.

[32] V. Franco, T. Gottschall, K.P. Skokov, O. Gutfleisch, First-Order Reversal Curve (FORC) analysis of magnetocaloric heusler-type alloys, IEEE Magn. Lett. 7 (2016), https://doi.org/10.1109/LMAG.2016.2541622.

[33] J. Rodríguez-Carvajal, Recent advances in magnetic structure determination by neutron powder diffraction, Phys. B: Phys. Condens. Matter 192 (1993) 55–69, https://doi.org/10.1016/0921-4526(93)90108-I.

[34] P. Álvarez-Alonso, J. López-García, G. Daniel-Perez, D. Salazar, P. Lázpita, J. P. Camarillo, H. Flores-Zuñiga, D. Rios-Jara, J.L. Sánchez-Llamazares, V. A. Chernenko, Simple set-up for adiabatic measurements of magnetocaloric effect, Key Eng. Mater. 644 (2015) 215–218, https://doi.org/10.4028/www.scientific.net/KEM.644.215.

[35] A. Quintana-Nedelcos, J.L. Sánchez Llamazares, C.F. Sánchez-Valdés, P. Álvarez Alonso, P. Gorria, P. Shamba, N.A. Morley, On the correct estimation of the magnetic entropy change across the magneto-structural transition from the Maxwell relation: study of MnCoGeBxalloy ribbons, J. Alloy. Compd. 694 (2017) 1189–1195, https://doi.org/10.1016/j.jallcom.2016.10.116.

[36] L.M. Moreno-Ramírez, V. Franco, Setting the basis for the interpretation of temperature first order reversal curve (TFORC) distributions of magnetocaloric materials, Met. (Basel) 10 (2020) 1–15, https://doi.org/10.3390/met10081039.

[37] ASTM Int., Standard Test Method for Transformation Temperature of Nickel-Titanium Alloys by thermal analysis, ASTM International, West Conshohocken, PA, 2009, https://doi.org/10.1520/F2004-05R10.2.

[38] V.K. Sharma, M.K. Chattopadhyay, R. Kumar, T. Ganguli, P. Tiwari, S.B. Roy, Magnetocaloric effect in Heusler alloys Ni50Mn 34In16 and Ni50Mn34Sn16, J. Phys. Condens. Matter 19 (2007), https://doi.org/10.1088/0953-8984/19/49/496207.

[39] B. Emre, S. Yüce, E. Stern-Taulats, A. Planes, S. Fabbrici, F. Albertini, L. Mañosa, Large reversible entropy change at the inverse magnetocaloric effect in Ni-Co-Mn-Ga-In magnetic shape memory alloys, J. Appl. Phys. 113 (2013) 213905, https://doi.org/10.1063/1.4808340.

[40] J.A. Blanco, D. Gignoux, D. Schmitt, Specific heat in some gadolinium compounds. II. Theoretical model, Phys. Rev. B 43 (1991) 13145–13151, https://doi.org/10.1103/PhysRevB.43.13145.

[41] V. Sánchez-Alarcos, V. Recarte, J.I. Pérez-Landazábal, E. Cesari, J.A. Rodríguez-Velamazán, Long-range atomic order and entropy change at the martensitic transformation in a Ni-Mn-In-Co metamagnetic shape memory alloy, Entropy 16 (2014) 2756–2767, https://doi.org/10.3390/e16052756.

[42] P. Álvarez-Alonso, C.O. Aguilar-Ortiz, J.P. Camarillo, D. Salazar, H. Flores-Zúñiga, V.A. Chernenko, Adiabatic magnetocaloric effect in Ni50Mn35In15 ribbons, Appl. Phys. Lett. 109 (2016) 212402, https://doi.org/10.1063/1.4968592.

[43] S.Y. Yu, A.J. Gu, S.S. Kang, S.J. Hu, Z.C. Li, S.T. Ye, H.H. Li, J.J. Sun, R.R. Hao, Large reversible magnetostrain in polycrystalline Ni50Mn33In17−xGax, J. Alloy. Compd. 681 (2016) 1–5, https://doi.org/10.1016/j.jallcom.2016.04.249.

[44] P. Lázpita, V.A. L'vov, J.R. Fernández, J.M. Barandiarán, V.A. Chernenko, Combined effect of magnetic field and hydrostatic pressure on the phase transitions exhibited by Ni-Mn-In metamagnetic shape memory alloy, Acta Mater. 193 (2020) 1–9, https://doi.org/10.1016/j.actamat.2020.04.008.

[45] C. Salazar Mejía, K. Mydeen, P. Naumov, S.A. Medvedev, C. Wang, M. Hanfland, A. K. Nayak, U. Schwarz, C. Felser, M. Nicklas, Suppression of the ferromagnetic order in the Heusler alloy Ni50Mn35In15 by hydrostatic pressure, Appl. Phys. Lett. 108 (2016) 261903, https://doi.org/10.1063/1.4954838.
[46] V.V. Sokolovskiy, V.D. Buchelnikov, S.V. Taskaev, V.V. Khovaylo, M. Ogura, P. Entel, Quaternary Ni-Mn-In-Y Heusler alloys: A way to achieve materials with better magnetocaloric properties? J. Phys. D. Appl. Phys. 46 (2013) 305003 https://doi.org/10.1088/0022-3727/46/30/305003.
[47] J.M. Barandiaran, V.A. Chernenko, E. Cesari, D. Salas, P. Lazpita, J. Gutierrez, I. Orue, Magnetic influence on the martensitic transformation entropy in Ni-Mn-In metamagnetic alloy, Appl. Phys. Lett. 102 (2013) 071904, https://doi.org/10.1063/1.4793412.
[48] C. Hao, M. Adil, J. Jiang, D. Duan, Thermal transformation arrest austenite in Ni-Co-Mn-In alloys within the martensite/strain-glass phase boundary, Phys. Lett. A 497 (2024) 129329, https://doi.org/10.1016/j.physleta.2024.129329.
[49] X. Moya, L. Mañosa, A. Planes, S. Aksoy, M. Acet, E.F. Wassermann, T. Krenke, Cooling and heating by adiabatic magnetization in the Ni50Mn34In16 magnetic shape-memory alloy, Phys. Rev. B 75 (2007) 184412, https://doi.org/10.1103/PhysRevB.75.184412.
[50] T. Gottschall, On the Magnetocaloric Properties of Heusler Compounds: Reversible, Time- and Size-dependent Effects of the Martensitic Phase Transition, Technische Univsersität Darmstadt, 2016. ⟨http://tuprints.ulb.tu-darmstadt.de/5582⟩.
[51] V.V. Khovaylo, K.P. Skokov, O. Gutfleisch, H. Miki, R. Kainuma, T. Kanomata, Reversibility and irreversibility of magnetocaloric effect in a metamagnetic shape memory alloy under cyclic action of a magnetic field, Appl. Phys. Lett. 97 (2010) 052503, https://doi.org/10.1063/1.3476348.
[52] K.P. Skokov, V.V. Khovaylo, K.-H. Müller, J.D. Moore, J. Liu, O. Gutfleisch, Magnetocaloric materials with first-order phase transition: thermal and magnetic hysteresis in LaFe11.8Si1.2 and Ni2.21Mn0.77Ga1.02, J. Appl. Phys. 111 (2012) 07A910, https://doi.org/10.1063/1.3670987.
[53] C. Salazar-Mejía, V. Kumar, C. Felser, Y. Skourski, J. Wosnitza, A.K. Nayak, Measurement-protocol dependence of the magnetocaloric effect in Ni-Co-Mn-Sb Heusler Alloys, Phys. Rev. Appl. 11 (2019) 054006, https://doi.org/10.1103/PhysRevApplied.11.054006.
[54] J. Liu, N. Scheerbaum, J. Lyubina, O. Gutfleisch, Reversibility of magnetostructural transition and associated magnetocaloric effect in Ni-Mn-In-Co, Appl. Phys. Lett. 93 (2008) 102512, https://doi.org/10.1063/1.2981210.
[55] A. Díaz-García, L.M. Moreno-Ramírez, J.Y. Law, F. Albertini, S. Fabbrici, V. Franco, Characterization of thermal hysteresis in magnetocaloric NiMnIn Heusler alloys by temperature first order reversal curves (TFORC), J. Alloy. Compd. 867 (2021) 159184, https://doi.org/10.1016/j.jallcom.2021.159184.
[56] J. Liu, T. Gottschall, K.P. Skokov, J.D. Moore, O. Gutfleisch, Giant magnetocaloric effect driven by structural transitions, Nat. Mater. 11 (2012) 620–626, https://doi.org/10.1038/nmat3334.
[57] A.P. Kazakov, V.N. Prudnikov, A.B. Granovsky, A.P. Zhukov, J. Gonzalez, I. Dubenko, A.K. Pathak, S. Stadler, N. Ali, Direct measurements of field-induced adiabatic temperature changes near compound phase transitions in Ni-Mn-In based Heusler alloys, Appl. Phys. Lett. 98 (2011) 131911, https://doi.org/10.1063/1.3574088.
[58] I. Dubenko, T. Samanta, A. Quetz, A. Kazakov, I. Rodionov, D. Mettus, V. Prudnikov, S. Stadler, P. Adams, J. Prestigiacomo, A. Granovsky, A. Zhukov, N. Ali, The comparison of direct and indirect methods for determining the magnetocaloric parameters in the Heusler alloy Ni 50Mn 34.8In 14.2B, Appl. Phys. Lett. 100 (2012) 192402, https://doi.org/10.1063/1.4714539.
[59] I. Titov, M. Acet, M. Farle, D. González-Alonso, L. Mañosa, A. Planes, T. Krenke, Hysteresis effects in the inverse magnetocaloric effect in martensitic Ni-Mn-In and Ni-Mn-Sn, J. Appl. Phys. 112 (2012) 1–6, https://doi.org/10.1063/1.4757425.
[60] M. Ghorbani Zavareh, C. Salazar Mejía, A.K. Nayak, Y. Skourski, J. Wosnitza, C. Felser, M. Nicklas, Direct measurements of the magnetocaloric effect in pulsed magnetic fields: the example of the Heusler alloy Ni50Mn35In15, Appl. Phys. Lett. 106 (2015) 071904, https://doi.org/10.1063/1.4913446.
[61] V.A. Chernenko, J.M. Barandiarán, J. Rodriguez Fernández, D.P. Rojas, J. Gutiérrez, P. Lázpita, I. Orue, Magnetic and magnetocaloric properties of martensitic Ni2Mn1.4Sn0.6 Heusler alloy, J. Magn. Magn. Mater. 324 (2012) 3519–3523, https://doi.org/10.1016/j.jmmm.2012.02.080.